Research Article

Felix Ellwanger*, Christos K. Georgantopoulos, Heike P. Karbstein, Manfred Wilhelm, and M. Azad Emin

Application of the ramp test from a closed cavity rheometer to obtain the steady-state shear viscosity $\eta(\dot{\gamma})$

https://doi.org/10.1515/arh-2022-0149
received December 22, 2022; accepted March 28, 2023

Abstract: The steady-state shear viscosity $\eta(\dot{\gamma})$ is required in controlling processing parameters for the extrusion processing of polymer melts. A new method, the so-called *ramp test*, is investigated in this study to obtain the steady-state shear viscosity with a closed cavity rheometer (CCR). To verify the method and the accuracy of the CCR data, three commercial polyolefin polymers, a low-density polyethylene (LDPE), a linear low-density polyethylene (LLDPE), and a polybutadiene (PBD), were used as model systems. Measurements of the magnitude of the complex viscosity $|\eta^*(\omega)|$ were compared with the steady-state shear viscosity data obtained by capillary rheometer and CCR. Further, time–temperature superposition master curves of the magnitude of the complex viscosity and steady-state shear viscosity obtained by CCR were developed for LLDPE and PBD. The influence of the cavity sealing on the instrument's accuracy to obtain the steady-state shear viscosity was investigated using the finite element method simulations. Thus, it was shown that the ramp test performed by CCR is a practical method to determine reliable and reproducible data of the steady-state shear viscosity within a wide range of temperatures (T = 50–180°C) for low and high viscous materials ($|\eta^*(\omega)|$ = 1.6–480 kPa s, M_w = 144–375 kg mol^{-1}).

Keywords: steady-state shear viscosity, closed cavity rheometer, ramp test, time–temperature superposition, numerical simulation

1 Introduction

Screw extrusion processing is a common process used to produce films, chemicals, and tires as well as food products such as pasta, cereals, or meat substitutes. For all these processes, the rheological behavior of the material used has a crucial role at various levels. This includes process control and stability as well as product properties and mechanical performance. Therefore, there is a significant effort to measure the rheological properties of the materials used under processing conditions in shear and elongation flows. Among others, the steady-state shear viscosity $\eta(\dot{\gamma})$ is of high interest, as it determines the torque required for extrusion. In addition, the mechanical stress profile during extrusion and the temperature reached in the screw section depend on the steady-state shear viscosity due to viscous heating [1]. In the die section, the steady-state shear viscosity also determines the flow conditions. Therefore, steady-state shear viscosity is of great interest for the control of extrusion processing for polymers [2–4] and for food products, i.e., meat replacers [5–7].

The viscosity of a fluid is the flow resistance force caused by the internal friction of the molecules [8]. Using a rotational rheometer, two different viscosities can be obtained depending on the measuring procedure. On the one hand, in the linear regime, the magnitude of the complex viscosity $|\eta^*(\omega)|$ can be obtained by applying

* **Corresponding author: Felix Ellwanger,** Karlsruhe Institute of Technology (KIT), Institute of Process Engineering in Life Sciences, Chair of Food Process Engineering (LVT), Gotthard-Franz-Straße 3, 76131 Karlsruhe, Germany, e-mail: felix.ellwanger@kit.edu
Christos K. Georgantopoulos: VAT Vakuumventile AG, Material and Manufacturing Technology, Core Technology, Seelistrasse 1, 9469 Haag, Switzerland
Heike P. Karbstein: Karlsruhe Institute of Technology (KIT), Institute of Process Engineering in Life Sciences, Chair of Food Process Engineering (LVT), Gotthard-Franz-Straße 3, 76131 Karlsruhe, Germany
Manfred Wilhelm: Karlsruhe Institute of Technology (KIT), Institute of Chemical Technology and Polymer Chemistry (ITCP), Engesserstraße 18, 76131 Karlsruhe, Germany
M. Azad Emin: Karlsruhe Institute of Technology (KIT), Institute of Process Engineering in Life Sciences, Chair of Food Process Engineering (LVT), Gotthard-Franz-Straße 3, 76131 Karlsruhe, Germany; nexnoa GmbH, Aachener Straße 1042, 50858 Köln, Germany

a small amplitude oscillatory shear (SAOS) flow. The magnitude of the complex viscosity $|\eta^*(\omega)|$ is defined as $|\eta^*(\omega)| = \sqrt{G'^2 + G''^2}/\omega$, where G' is the storage modulus, G'' is the loss modulus, and ω is the angular frequency. On the other hand, in the nonlinear regime, the steady-state shear viscosity $\eta(\dot{\gamma})$ is defined as $\eta(\dot{\gamma}) = \sigma(\dot{\gamma})/\dot{\gamma}$, where $\dot{\gamma}$ is the shear rate and $\sigma(\dot{\gamma})$ is the shear stress. The complex viscosity $|\eta^*(\omega)|$ and the steady-state shear viscosity $\eta(\dot{\gamma})$ are linked via the empirical Cox–Merz rule, which is widely used in the industry [9]. The rule originally established by Cox and Merz showed that the magnitude of the complex viscosity $|\eta^*(\omega)|$ obtained by a rotational rheometer is very close to the apparent shear viscosity $\eta_{app}(\dot{\gamma})$ measured by capillary rheometer, for equality of the frequency ω and the steady-state shear rate $\dot{\gamma}$ ($|\eta^*(\omega)| = \eta_{app}(\dot{\gamma})$ for $\dot{\gamma} = \omega$). The applicability of the Cox–Merz rule to the steady-state shear viscosity $\eta(\dot{\gamma})$ and the magnitude of the complex viscosity $|\eta^*(\omega)|$ has been established for many polymer melts, concentrated systems, and semi-dilute systems ($|\eta^*(\omega)| = \eta(\dot{\gamma})$ for $\dot{\gamma} = \omega$). For example, a detailed investigation on the appraisal of the Cox–Merz rule for polyolefin melts can be found in the work of Snijkers and Vlassopoulos [10].

Furthermore, the comparison of the steady-state shear stress $\sigma(\dot{\gamma})$ and the magnitude of the complex shear modulus $|G^*(\omega)|$ ($\sigma(\dot{\gamma}) = |G^*(\omega)|$ for $\dot{\gamma} = \omega$) proposed by Winter is used to draw an additional conclusion about the viscoelasticity of the investigated material [11]. Since the Cox–Merz rule is an empirical rule for which no final justification has been provided, it is not recommended to use the magnitude of the complex viscosity to predict the steady-state shear viscosity for unknown materials. In the context of this publication, it is assumed that the Cox–Merz rule is typically valid within a 15% deviation between the magnitude of the complex viscosity and the steady-state shear viscosity. This assumption is made to cover possible measurement inaccuracies of the different devices and measurement routines used.

Modern rheometers can provide reliable information on the magnitude of the complex viscosity, but it is still challenging to obtain reliable data on the steady-state shear viscosity for strongly viscoelastic materials. Typical advantages and disadvantages to obtain the steady-state shear viscosity are given in Table 1. In this context, it would be of interest, for both research purposes and industry, to have a fast and accurate method that requires the use of only a small amount of material to obtain the steady-state shear viscosity for strongly viscoelastic materials.

As Table 1 displays, closed cavity rheometers (CCRs) have a great potential for determining the steady-state shear viscosity compared to the capillary and open cavity rheometers. CCRs are usually equipped with a motor providing higher torque values, which enables the measurement of a high viscous material without using small geometries ($r < 5$ mm). By applying and controlling pressure, and using plates with grooves, wall slippage can be prevented. The closed cavity set up of the CCR is eliminating the edge fracture. In addition, by the application of pressure in the closed cavity, the evaporation of solvents, i.e., water at high temperatures is avoided. A small

Table 1: Advantages, disadvantages, and typical limitations of open cavity rheometers, capillary rheometers, and CCR

	Open cavity oscillatory rheometer	Capillary rheometer	Closed cavity oscillatory rheometer
Advantages	Low amount of material needed (1 g), versatile in measuring procedures, fast temperature control (30 K/min)	Feasibility of high shear rates ($\dot{\gamma} > 100\ s^{-1}$), comparable with actual extrusion processes	Low amount of material needed (4.5 g), versatile in measuring procedures, fast temperature control (80 K/min), no edge fracture, pressure regulation
Disadvantages	Wall slippage, secondary flow, edge fracture, loss of lubricant/solvent	Different flow types (Couette vs Poiseuille) to compare it with rotational rheometer, wall slippage, data correction needed, large amount of material needed (>100 g), viscous heating, extrusion flow instabilities, not suitable for low shear rates	No continuous rotation, Not suitable for low viscous material, Wall slippage, Little variety of measurement geometries
Typical limitations (shear rate, temperature, torque/force)	$\dot{\gamma} = 0.001–1,000\ s^{-1}$, $T = -150$ to 600°C, $M = 0.1$ µNm to 0.2 Nm	$\dot{\gamma} = 10–10,000\ s^{-1}$, $T = 25–600$°C, $F = 10–50$ kN	$\dot{\gamma} = 0.01–30\ s^{-1}$, $T = 25–230$°C, $M = 0.1$ mNm to 25 Nm

chamber geometry ($r \approx 20$ mm) allows a quick and accurate increase or decrease of test temperature. These rheometers are widely used to determine viscoelastic properties of rubbers and water-containing food samples [12–14]. A measurement of the steady-state shear viscosity with the CCR would therefore offer the possibility of carrying out quick, simple measurements without having to use a lot of material.

To the best of our knowledge, Burhin and Rauschmann [15–17] as well as Heyer et al. [18] are the only authors to have published on determining steady-state shear viscosity data with CCR. In their work, the ramp test method, a method to obtain the steady-state shear viscosity via CCR, was introduced and mainly used to investigate the steady-state shear viscosity of rubbers. In addition, they used the ramp test in combination with a polished plate to obtain information about wall slippage. Most recently, Rauschmann et al. presented a new generation of CCR (Rubber Process Analyzer Ultra, Bareiss Prüfgerätebau GmbH, Oberdischingen, Germany), which enables continuous rotation at shear rates up to $\dot{\gamma} = 500\ s^{-1}$ [19].

To further verify the ramp test method, this study presents data for a low-density polyethylene (LDPE), a linear low-density polyethylene (LLDPE), and polybutadiene (PBD). The specific choice of materials was made to present results from well-known, widely used polymers. Also, by choosing these polymers as samples, a wide range of average molecular weights and processing behaviors are investigated. Hence, in comparison to the filled system used in the previous studies, thorough conclusions by using simpler samples can be drawn about the ramp test method. First, data obtained by SAOS measurements were compared with steady-state data obtained by capillary measurements to validate the applicability of the Cox–Merz rule. The data of the magnitude of the complex viscosity for the three polymers were fitted by the Cross model [20]. The Cross model found for LDPE was used for numerical finite element simulations to investigate the theoretical influence of the cavity sealing on the CCR's accuracy. Subsequently, measurements were performed with the CCR to obtain the steady-state shear viscosity of the same LDPE, LLDPE, and PBD.

To demonstrate the potential of the ramp test and the accuracy of the CCR, SAOS and steady-state shear measurements were carried out for LLDPE and PBD at different temperatures. The data obtained were used to construct master curves using the time–temperature superposition (TTS) principle [21]. The horizontal a_T and vertical b_T shifting factors were chosen based on the SAOS measurements and could be used for both the magnitude of the complex viscosity and the steady-state shear viscosity data.

2 Materials

The materials used in this study were LDPE, LLDPE, and PBD. The melting temperature and the molecular characteristics (number average molecular weight M_n, average molecular weight M_w, and polydispersity $Đ\left(\frac{M_n}{M_w}\right)$ are listed in Table 2. The molecular characteristics of LDPE and LLDPE have been obtained by a high-temperature size exclusion chromatography (SEC) coupled with a multi-angle laser light scattering technique at $T = 140$°C. Linear polyethylene (PE) standards were used for column calibration. The molecular weight distribution of the investigated PBD was detected by the size exclusive chromatography equipped with a differential refractive index detector. Homopolymer PBD standards with linear molecular architecture were used for column calibration.

3 Experimental and computational rheological measurements

3.1 The magnitude of the complex viscosity $|\eta^*(\omega)|$

To determine the magnitude of the complex viscosity $|\eta^*(\omega)|$, frequency sweep experiments were performed with a CCR, also called rubber process analyzer (RPA) flex, from TA Instruments, Inc. (New Castle, DE, USA),

Table 2: Melting temperature and molecular characteristics of the investigated LDPE, LLDPE, and PBD

	Melting temperature (°C)	Glass transition temperature (°C)	M_n (kg mol^{-1})	M_w (kg mol^{-1})	$Đ$
LDPE	114	—	23.7	146	6.16
LLDPE[a]	125	—	32.7	144	4.40
PBD[b]	—	–108	107	375	3.50

[a]Adapted from Georgantopoulos et al. [22]. [b]Adapted from Georgantopoulos et al. [3].

as shown in Figure 1. The CCR is equipped with a grooved cone-cone geometry (r = 20.625 mm, Θ = 7.16°). The grooves in the cones are used to prevent wall slippage. The experiments were carried out within the linear viscoelastic regime (LVE) in an angular frequency range between $\omega = 0.05^{-1}$ and 315 rad s^{-1}. The strain sweeps performed to determine the LVE range are shown in Figure S3 in the supplementary material. For LDPE and LLDPE, a strain of $\gamma = 10\%$, and for PBD, a strain of $\gamma = 1\%$ was chosen to obtain an accurate signal in the low-frequency range. Before each measurement, the material was held at the zero position for 3 min to ensure a homogenous temperature profile. Measurements were performed at least in duplicate to determine measurement errors.

3.2 Steady-state shear viscosity $\eta(\dot{\gamma})$

To determine the steady-state shear viscosity $\eta(\dot{\gamma})$ via different methods, experiments were performed with the aforementioned CCR and a capillary rheometer Göttfert RG 50 from Göttfert Werkstoff-Prüfmaschinen GmbH (Buchen, Germany).

For the capillary rheometer experiments, the sample was loaded in the capillary rheometer reservoir (30 mm reservoir diameter) and remained there for 15 min to ensure a homogenous temperature profile. In total, three commercial round capillary dies (with circular cross-section area) with a length of L = 30, 20, and 10 mm and a diameter of D = 2 mm were used. The raw data were corrected according to Bagley [24] and Rabinowitsch [25].

For the CCR, the material was held at a zero position for 3 min to ensure a homogenous temperature profile. The lower cone then deflects by a maximum of γ = 50 (almost one rotation) at a constant rotational speed, while the torque is measured at the upper cone. This type of experiment is also known as a start-up shear experiment and is used to obtain the steady-state shear viscosity for open cavity rheometers [26,27]. After the full displacement, the lower cone rotates back into the zero position. The steady-state shear viscosity $\eta(\dot{\gamma})$ can then be calculated by equation (1), where σ is the shear stress, $\dot{\gamma}$ is the shear rate, M_{up} is the torque at the upper cone, and r is the radius of the cone.

$$\eta(\dot{\gamma}) = \frac{\sigma}{\dot{\gamma}} = \frac{3 \cdot M_{up}}{2 \cdot \pi \cdot r^3} \cdot \frac{1}{\dot{\gamma}}. \quad (1)$$

This study has run two routines in which the steady-state shear viscosity of the sample is measured in 13 consecutive deflections. The rotational speed during deflection was chosen so that the shear rate was between $\dot{\gamma}$ = 0.1 and 30 s^{-1}. Lower shear rates could not be achieved due to a poor signal-to-noise ratio. Higher shear rates could not be achieved due to limitations of the limited rotation velocity of the instruments motor. Measurements were made from low to high shear rate and in reverse. Due to the grooved plates of the geometry, it was initially assumed that slippage was prevented and that the true steady-state shear viscosity was directly obtained without any further correction.

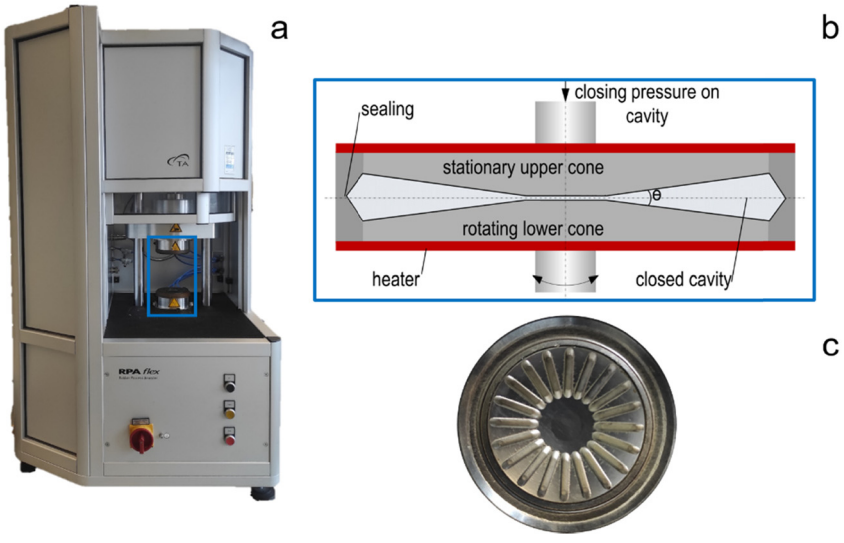

Figure 1: CCR named as RPA by TA Instruments. (a) CCR, (b) function sketch closed cavity [23], and (c) grooved lower cone.

3.3 Viscosity model

The magnitude of the complex viscosity $|\eta^*(\omega)|$ as a function of angular frequency ω was fitted with a Cross model, given by equation (2):

$$|\eta^*(\omega)| = \frac{|\eta_0^*|}{1 + (\tau \cdot \omega)^n}, \tag{2}$$

where $|\eta_0^*|$ is the zero-shear viscosity, τ is the relaxation time, and n is the power-law index.

3.4 Numerical simulation

The calculation of the numerical equations was performed with ANSYS POLYFLOW® 2020 R2 by Ansys Inc. (Canonsburg, PA, USA), which provides a finite element solver for highly viscous media. The program is mainly used in the field of extrusion, for both screw extrusion and flow through dies [5,28–30]. The simulated computational domain represents the CCR; see Figure 2a–c. The geometric dimensions were taken from the publication of Leblanc and Mongruel [31]. To verify the simulations and to further investigate the influence of the sealing, a simplified open cavity rheometer was also considered; see Figure 2d. The grooves of the geometry have been omitted to simplify mesh generation. The influence of the grooves on the shear rate may influence the accuracy, but it is not investigated in this study.

The mesh is depicted in Figure 2a, c, and d and is a structured mesh, which becomes finer toward the two contact surfaces: polymer-cones and polymer-sealing. A computational mesh with 147,240 elements for the cavity and 22,140 elements for each cone was proven not to affect the simulation results numerically. To take the rotation of the lower cone and the torque measurement at the upper cone into account, the mesh superposition technique introduced by Avalosse was used [29]. In this calculation technique, the mesh for the flow domain and the rotating/stationary parts are superimposed. For the CCR, the mesh of the lower rotating cone and the mesh of the upper stationary cone were superimposed on the mesh of the cavity. While solving the Navier–Stokes equations, a step function was added to check whether an element is in the flowed-through domain (cavity) or the rotating/stationary part (cone). If an element is in the flowed-through domain, the Navier–Stokes equations were solved. Otherwise, the velocity of the rotating/stationary body was assumed. Further information about this simulation method can be found elsewhere [28,29]. A no-slip boundary condition was assumed at the surface between the cone and the cavity. This is justified due to the usage of grooved cones in the experimental investigation. For the surface between the cavity and the sealing, the no-slip boundary condition and the free-slip boundary condition were investigated. For the simplified open cavity rheometer, the open cavity surface was described as a free-slip boundary condition. The energy equation, and thus the temperature of the material, was not taken into calculation. Assuming that the Cox–Merz rule is valid for the investigated LDPE, the steady-state shear viscosity of the material is described by a Cross model (equation (2)), which has been used to fit the experimental SAOS data (Figure 3a).

Mini-elements for velocity and linear pressure were chosen as interpolation settings. Iterations with a Picard scheme were performed, to take the viscosity implemented

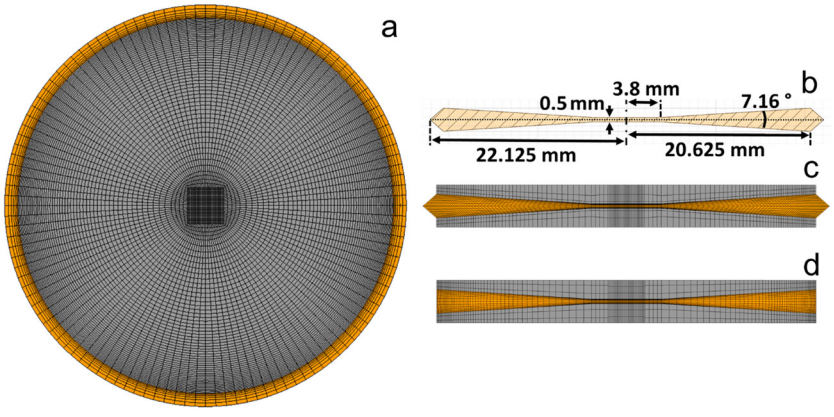

Figure 2: Geometry and mesh for the simulation of the CCR (orange = fluid domain, gray = rotating lower cone and stationary upper cone). (a) Top view, (b) technical drawing of the closed cavity, (c) cross-section CCR with the used computational mesh, and (d) cross-section simplified open cavity rheometer with the used computational mesh.

via a Cross model into account. To take the influence of the shear rate into account, a simulation with 25 different rotational speeds ($\dot{\gamma} = 10^{-3}$ to $10^{3}\ s^{-1}$) was carried out for the CCR at each boundary condition of the sealing-cavity surface and the simplified open cavity rheometer. The results were used to examine the actual shear rate distribution between the cones and near the sealing. In addition, the torque at the upper cone was determined, and the steady-state shear viscosity was calculated using equation (1). Simulations were performed on a cluster server, computing one node with 32 Intel Xeon Gold 6230 processors and 70 GB of RAM.

4 Results and discussion

4.1 Investigation of the magnitude of the complex viscosity $|\eta^*(\omega)|$ and steady-state shear viscosity $\eta(\dot{\gamma})$ of the different polymers

The magnitude of the complex viscosity $|\eta^*(\omega)|$ of the LDPE, LLDPE, and PBD samples was obtained by using the CCR. The data were then compared with data of the steady-state shear viscosity $\eta(\dot{\gamma})$ obtained by a capillary

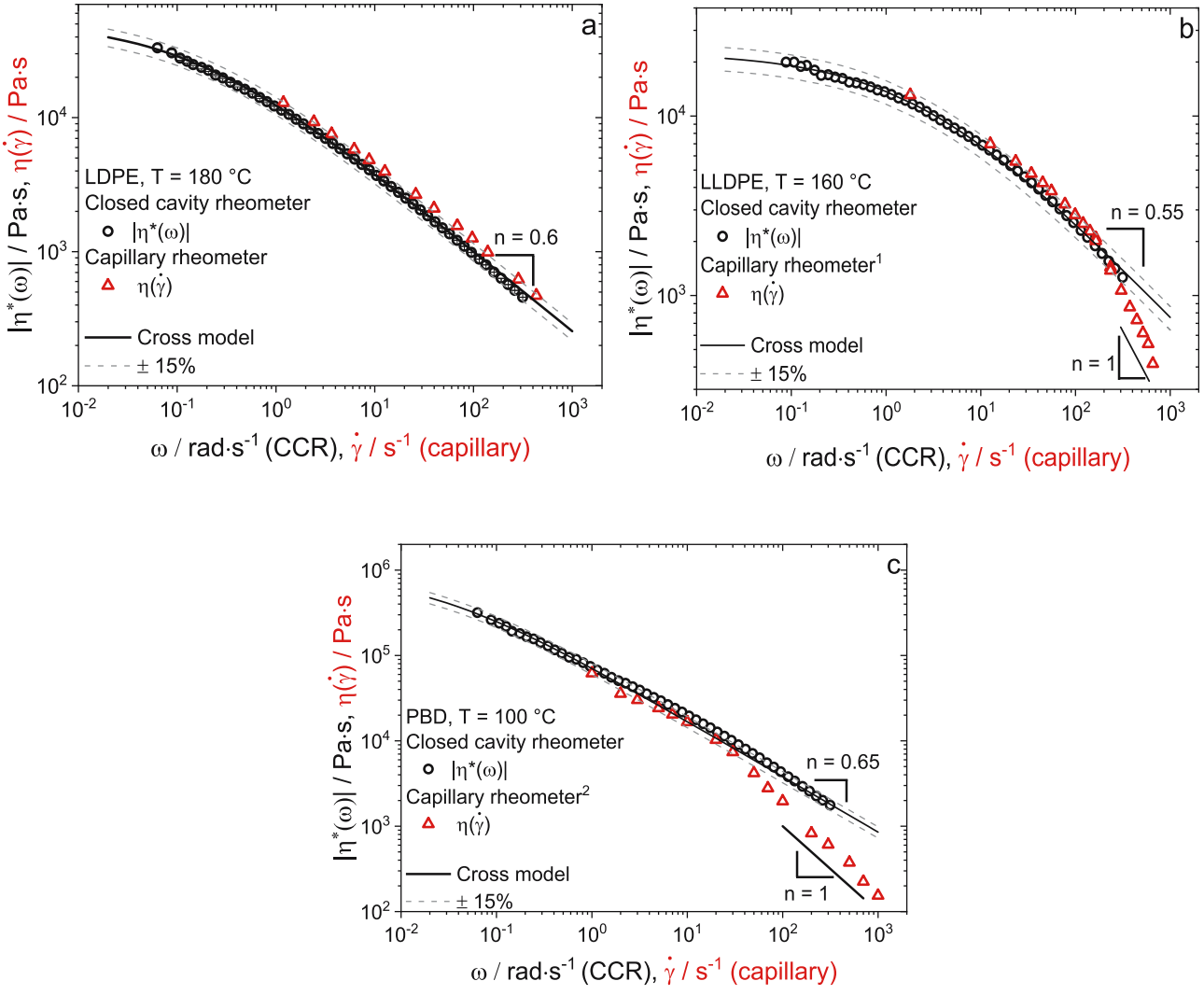

Figure 3: The magnitude of the complex viscosity $|\eta^*(\omega)|$ as a function of angular frequency ω obtained by SAOS measurements with the CCR and the steady-state shear viscosity $\eta(\dot{\gamma})$ as a function of shear rate $\dot{\gamma}$ obtained by the capillary rheometer, corrected by Bagley and Weißenberg-Rabinowitsch for (a) LDPE at $T = 180°C$ and (b) LLDPE at $T = 160°C$ ([1]steady-state shear viscosity data adapted from Georgantopoulos et al. [22]; Figure 7a and c) PBD at $T = 100°C$ ([2]steady-state shear viscosity data adapted from Georgantopoulos et al. [3]; Figure 9c).

rheometer Göttfert RG50. To obtain the magnitude of the complex viscosity, SAOS measurements were performed at typical processing temperatures of $T = 180°C$ for LDPE, $T = 160°C$ for LLDPE, and $T = 100°C$ for PBD in the linear viscoelastic region. In Figure 3a–c, the magnitude of the complex viscosity $|\eta^*(\omega)|$ is plotted as a function of the angular frequency ω, and the steady-state shear viscosity $\eta(\dot{\gamma})$ is plotted as a function of the shear rate $\dot{\gamma}$, black and red symbols, respectively. For the considered range of $\omega = 0.05–315\,\mathrm{rad\,s^{-1}}$, a shear-thinning behavior with a slope of $n = 0.6$ for LDPE, $n = 0.55$ for LLDPE, and $n = 0.65$ for PBD can be observed. In the low-frequency range ($\omega < 1\,\mathrm{rad\,s^{-1}}$), a change in the slope can be observed, indicating the start of the zero shear viscosity plateau. The shear-thinning behavior is typical of polymers and is well known for LDPE, LLDPE, and PBD. The Cross model (equation (2)) was suitable to describe the data of the SAOS measurements. The Cross model fitting parameters for LDPE, LLDPE, and PBD are listed in Table 3. The zero shear viscosity of the different polymers was estimated as it was not in the shear rate range studied and is not of interest for this investigation. To assess whether the Cox–Merz rule applies to the three commercial polymers, a 15% deviation was added to the Cross model (dashed gray lines). The assumption that the Cox–Merz rule applies despite a 15% deviation was made to consider possible measurement inaccuracies of the devices and measurement routines used. In particular, data obtained by the capillary rheometer can be affected by slippage, viscous heating, pressure effects, and other instabilities (Table 1).

To prove the applicability of the Cox–Merz rule, data for the steady-state shear viscosity of LLDPE and PBD were taken from the literature [3,22]. To obtain data for the steady-state shear viscosity of LDPE, measurements were carried out with a capillary rheometer. The data were corrected to Bagley and Weißenberg-Rabinowitsch correction as given in Hatzikiriakos and Migler [32]. Consequently, the steady-state shear viscosity $\eta(\dot{\gamma})$ is plotted against the shear rate $\dot{\gamma}$ in Figure 3a–c (red triangles). The steady-state data for the LDPE (Figure 3a) shows a shear thinning behavior with a slope of $n = 0.6$ for the entire measuring range. The values are about 15% higher than the values of the magnitude of the complex viscosity. Therefore, in the context of this investigation, it can still be assumed that the Cox–Merz rule applies in the investigated shear rate range. It is not a common observation that the steady-state shear viscosity exceeds the values of the magnitude of the complex viscosity, but this has been reported for LDPE samples in the literature [10,33]. However, there is experimental evidence that shows an agreement of the viscosities for a LDPE sample and thus validity of the Cox–Merz rule [34].

For the LLDPE at $T = 160°C$ (Figure 3b), a shear thinning behavior with a slope of $n = 0.55$ can be found up to shear rates of $\dot{\gamma} = 163\,\mathrm{s^{-1}}$. In this range, the steady-state shear viscosity is within the 15% deviation of the Cross model found for the magnitude of the complex viscosity. Thus, it can be assumed that the Cox–Merz rule is valid within a 15% deviation in the shear rate range of $\dot{\gamma} = 2–163\,\mathrm{s^{-1}}$ at $T = 160°C$. The steady-state shear viscosity for shear rates above $\dot{\gamma} = 163\,\mathrm{s^{-1}}$ shows a decrease in the slope up to a slope of $n = 1$. A decrease in the slope of the shear-thinning behavior is often reported in the context of capillary rheometer measurements of polymer melts and is mainly related to wall slippage [4,35–37]. Accordingly, it is assumed here that the deviation is due to wall slippage.

The steady-state data for PBD at $T = 100°C$ (Figure 3c) show a shear thinning behavior with a slope of $n = 0.65$ up to a shear rate of $\dot{\gamma} = 20\,\mathrm{s^{-1}}$. Up to this shear rate, the steady-state shear viscosity is below but within the 15% deviation of the Cross model found for the SAOS measurements, except for an outlier at $\dot{\gamma} = 2\,\mathrm{s^{-1}}$. For shear rates higher $\dot{\gamma} = 20\,\mathrm{s^{-1}}$, a decreasing slope up to a slope of $n = 1$ can be seen. As already described for the LLDPE, a decreasing slope can be related to wall-slippage. Thus, it is assumed that the Cox–Merz rule is applicable within a 15% deviation for the investigated PBD and the deviation at shear rates higher $\dot{\gamma} = 20\,\mathrm{s^{-1}}$ is due to wall-slippage.

Table 3: Fitting parameters of the Cross model under the following conditions: (a) LDPE at $T = 180°C$; (b) LLDPE at $T = 140$, 160, and 180°C; and (c) PBD at $T = 50$, 100, and 150°C

$$|\eta^*(\omega)| = \frac{|\eta_0^*|}{1 + (\tau \cdot \omega)^n}$$

	T (°C)	$\lvert\eta_0^*\rvert$ (kPa s)	τ (s)	n (–)
LDPE	180	52	7	0.6
LLDPE	150	36	0.75	0.55
	160	22.5	0.45	0.55
	180	17.5	0.32	0.55
PBD	50	2,790	155	0.65
	100	930	47	0.65
	150	413	19	0.65

Here, $|\eta_0^*|$ is the zero shear viscosity, τ is the relaxation time, and n is the power-law index.

4.2 Numerical investigation of the influence of the cavity sealing on the accuracy of the CCR

To investigate the influence of the cavity sealing on the accuracy of the CCR to obtain the steady-state shear

viscosity, numerical investigations were performed. The possible influence of the grooves on the accuracy of the instrument was neglected. First, a simplified open cavity rheometer (Figure 2d) was simulated at constant rotational speed (shear rate $\dot{\gamma} = 1\,s^{-1}$). Then, simulations at different rotational speeds were performed. Since it is not clear whether the material adheres to the surface of the sealing or slides during experimental conditions, both the no-slip and free-slip boundary conditions were considered as two extremes for the simulation. In Figure 4a, the shear rate distribution between the cones is shown for (i) the open cavity rheometer, (ii) the CCR with no-slip conditions applied to the sealing, and (iii) the CCR with slip conditions applied on the sealing. The rotational speed was chosen so that a theoretical shear rate of $\dot{\gamma} = 1\,s^{-1}$ results. For the open cavity rheometer (Figure 4a(i)), a uniform shear rate distribution can be observed. Close to the rotation center, a decreasing shear rate can be found in all configurations in Figure 4a. This is typical for rotational rheometers equipped with cone and cone geometry.

The results of the CCR, shown in Figure 4a(ii) and (iii), indicate that the sealing can have an effect on the shear rate distribution, especially close to the sealing. For the simulation with no-slip conditions shown in Figure 4a(ii), an increase in the shear rate to a maximum of $\dot{\gamma} = 10.2\,s^{-1}$ can be observed at the edge of the rotating cone and seal. At the edge of the stationary upper cone, a decrease in the shear rate to a minimum of $\dot{\gamma} = 0.02\,s^{-1}$ is detected. The reduced shear rate extends to the tip of the sealing, where values of $\dot{\gamma} = 0.02\,s^{-1}$ can be observed. This influence of the sealing on the shear rate distribution has already been reported by Leblanc and Mongruel for a two-dimensional simulation of the CCR, and it is in agreement with our findings [31]. However, the present simulation results are more detailed due to the three-dimensional simulation and additionally the use of a non-Newtonian fluid. Therefore, accurate information about the influence of the sealing is given. For the simulation with the free-slip boundary condition (Figure 4a(iii)), the shear rate distribution is less influenced by the sealing. At the edges of the rotating lower cone and stationary upper cone, an increase in the shear rate to a maximum of $\dot{\gamma} = 2.3\,s^{-1}$ can be found. At the tip of the sealing, a minimum of $\dot{\gamma} = 0.1\,s^{-1}$ can be detected. Accordingly, it can be observed for both simulations that the shear rate is influenced at the edge of the upper cone. Thus, an influence on the torque measurement and finally the viscosity measurement cannot be excluded and is considered in the next section.

In Figure 4b, the steady-state shear viscosity $\eta(\dot{\gamma})$ determined in equation (1) is plotted against the shear rate $\dot{\gamma}$ for the different simulations. For the simulation with the open cavity rheometer (Figure 4a(i)), a deviation of less than 1% between the calculated steady-state shear viscosity and the implemented Cross model can be seen for all shear rates. This shows that the simulation is accurate enough to calculate the viscosity using equation (1). For the simulations with the no-slip boundary condition applied to the sealing, it can be observed that the steady-state shear viscosity is underestimated by equation (1). The deviation of the steady-state shear viscosity from the Cross model is between 11.5% for $\dot{\gamma} = 10^{-3}\,s^{-1}$ and 12.2% for $\dot{\gamma} = 10^{3}\,s^{-1}$. The underestimation of viscosity is caused

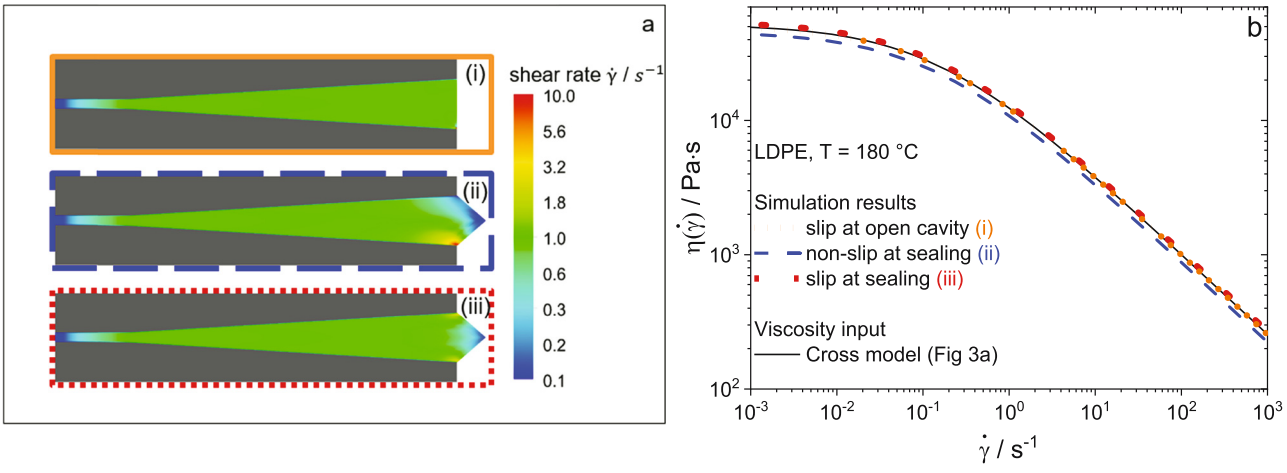

Figure 4: (a) Shear rate distribution between the rotating lower cone and stationary upper cone offset at $\dot{\gamma} = 1\,s^{-1}$ for (i) the simplified open cavity rheometer, (ii) the CCR with no-slip boundary conditions at the sealing, and (iii) the CCR with free-slip boundary conditions at the sealing. (b) Calculated steady-state shear viscosity $\eta(\dot{\gamma})$ data for the simplified open cavity rheometer (orange dotted line), CCR with no-slip boundary conditions at the sealing (blue dashed line), and CCR with free-slip boundary conditions at the sealing (red dotted line).

by the inhomogeneous shear rate distribution, which is a consequence of the no-slip conditions on the sealing. This reduces the shear stress close to the upper cone, resulting in a lower measured torque. The shear stress distribution between the cones can be seen in Figure S1 in the supplementary material for the same conditions shown in Figure 4a. The findings of the lowered shear rate, and thus, the underestimation of the viscosity are in agreement with the data of LeBlanc and Mongruel [31].

The steady-state shear viscosity $\eta(\dot{\gamma})$ calculated by equation (1) for the simulation data with the free-slip boundary condition at the sealing resulted in an overestimation of the steady-state shear viscosity of 5.9%. These findings can be attributed to the increased shear rate and correspondingly increased shear stress at the edges of the upper cone. In conclusion, the simulations with the different boundary conditions show that the error in the calculation of the viscosity with equation (1) should not exceed 12.2% due to instabilities caused by the sealing. Slippage effects at the rotating cone were not investigated in the simulation, but it can be assumed that these influence the accuracy of the results to a greater extent than slippage at the sealing.

4.3 Steady-state shear viscosity $\eta(\dot{\gamma})$ obtained by a CCR

The steady-state shear viscosity $\eta(\dot{\gamma})$ for the LDPE at a temperature of T = 180°C was obtained by experimental measurements with the CCR. By setting up different deflection times, different shear rates could be measured. In Figure 5a, the torque measured at the upper cone during one full deflection of γ = 50 is shown for the shear rates of $\dot{\gamma}$ = 1, 3, 10, and 30 s^{-1}. For all four shear rates, an increase in torque can be observed at the beginning (below γ = 15), leading to an overshoot before finally reaching a steady state. The overshoot is often observed in polymer melts and is attributed to the alignment of the polymer chains [38]. To determine the value of the plateau, the mean value of the torque in the range between γ = 30 and γ = 50 is calculated. To check whether this approach is legitimate, the mean value of the torque is determined for a window of every $\Delta\gamma$ = 5 deflection. We define the steady state to have been reached when the average value does not deviate by more than 1% compared to the previous value. Accordingly, for the curves shown in Figure 5a, the steady-state condition is reached after deflections of γ = 30 for $\dot{\gamma}$ = 30 s^{-1}, γ = 25 for $\dot{\gamma}$ = 10 s^{-1}, γ = 20 for $\dot{\gamma}$ = 3 s^{-1}, and γ = 15 for $\dot{\gamma}$ = 1 s^{-1}. These steady-state values were used to calculate the steady-state shear viscosity according to equation (1).

Figure 5b presents the steady-state shear viscosity $\eta(\dot{\gamma})$ and the magnitude of the complex viscosity $|\eta^*(\omega)|$ for the investigated LDPE at T = 180°C obtained by the CCR. In addition, the Cross model obtained by fitting the magnitude of the complex viscosity in Figure 3a is also depicted. To be able to estimate the deviation of the steady-state shear viscosity from the magnitude of the complex viscosity, a 15% deviation was added to the Cross model. The data of the steady-state shear viscosity, measured from low shear rates to high shear rates, overlaps with the Cross model for shear rates higher $\dot{\gamma}$ = 0.5 s^{-1} (red squares). The obtained data for shear rates

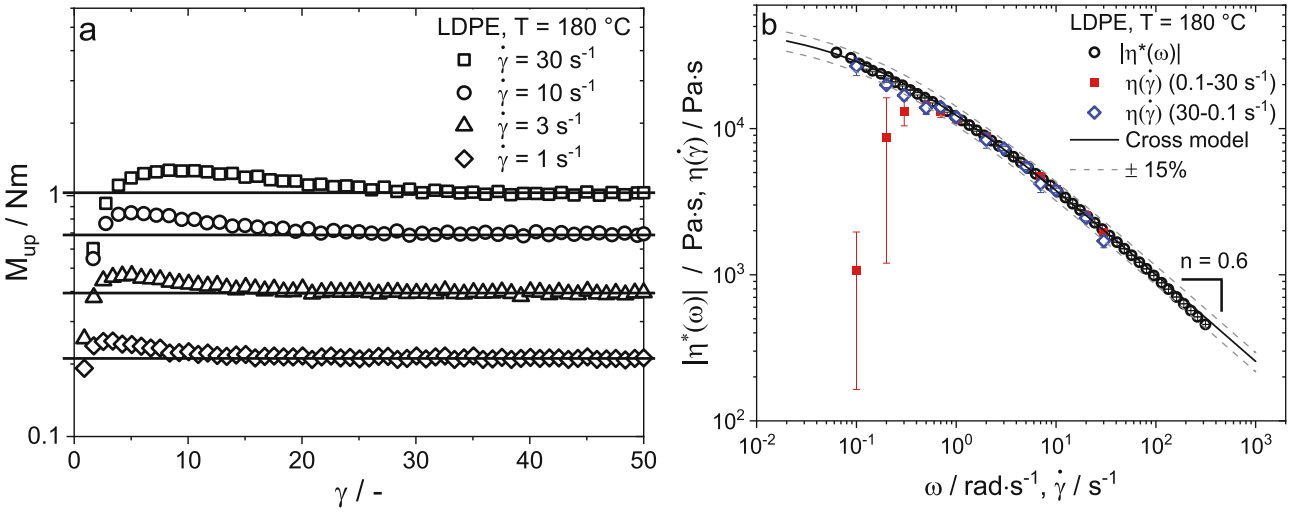

Figure 5: (a) Torque M_{up} as a function of strain γ for LDPE at the shear rate of $\dot{\gamma}$ = 1, 3, 10, and 30 s^{-1} and (b) the magnitude of the complex viscosity $|\eta^*(\omega)|$ as a function of angular frequency ω obtained by oscillatory shear frequency sweep experiments with rotational CCR and the steady-state shear viscosity $\eta(\dot{\gamma})$ as a function of shear rate $\dot{\gamma}$ obtained by rotational CCR.

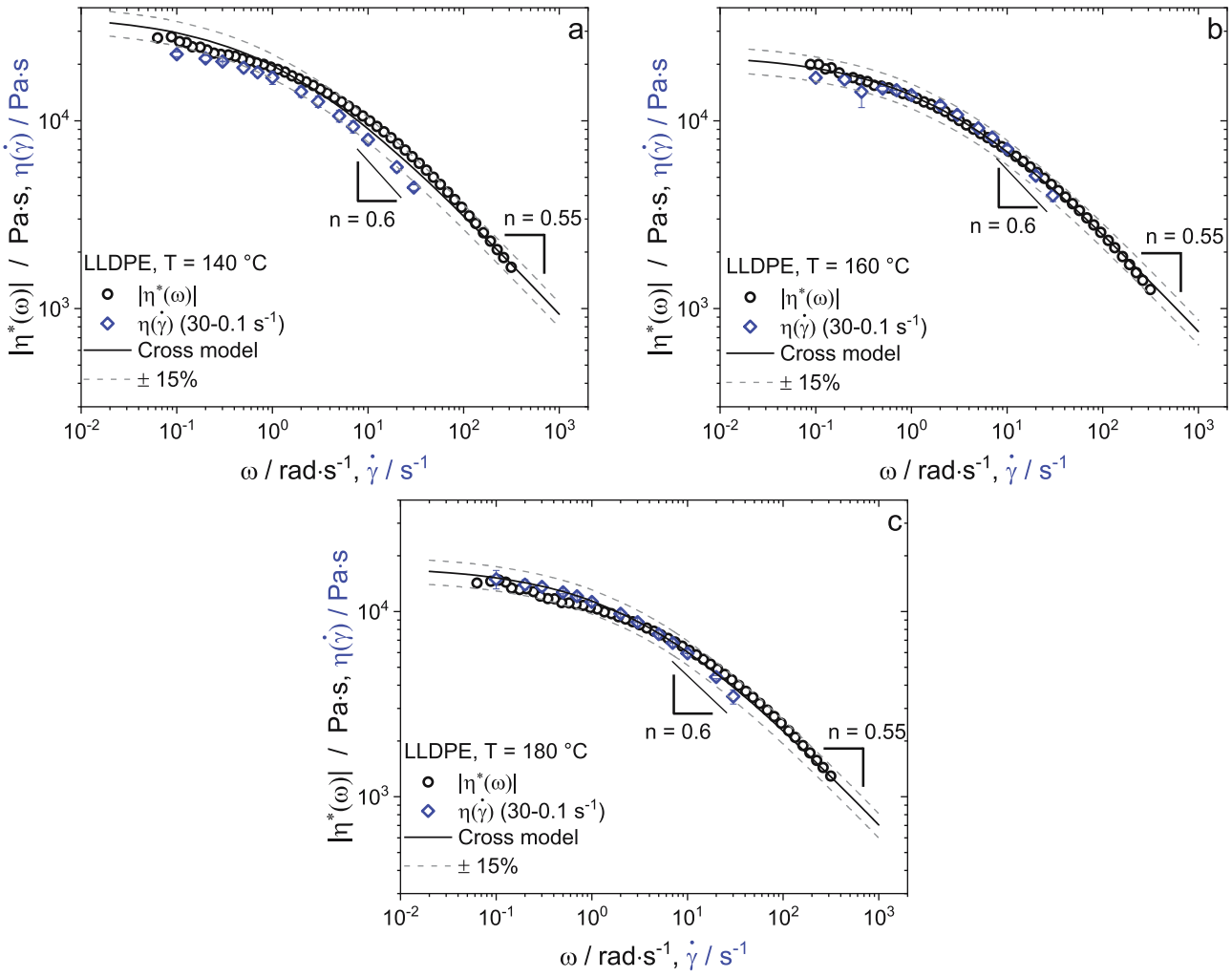

Figure 6: The magnitude of the complex viscosity $|\eta^*(\omega)|$ as a function of angular frequency ω obtained by oscillatory shear frequency sweep experiments with rotational CCR and the steady-state shear viscosity $\eta(\dot{\gamma})$ as a function of shear rate $\dot{\gamma}$ obtained by rotational CCR for LLDPE at (a) 140°C, (b) 160°C, and (c) 180°C.

of $\dot{\gamma} = 0.1$, 0.2, and 0.3 s^{-1} have deviations between 20 and 85% and are below the Cross model. For these data, a steady-state plateau could not be reached. Examples of using the measured torque for the triple determination at a shear rate of $\dot{\gamma} = 0.3\,s^{-1}$ are shown in the supplementary information. To calculate the steady-state shear viscosity for these shear rates, the mean value of the torque between a strain of $\gamma = 30$ and 50 was determined, regardless of whether a steady state was reached. Using the reversed measurement routine from high to low shear rates, the data of the steady-state shear viscosity are within the 15% deviation of the Cross model (blue rhombus). Based on these measurement data, the validity of the Cox–Merz rule can be assumed within a 15% deviation for the investigated LDPE. The data thus confirm the results of the measurements from the capillary rheometer (Figure 3a) and extend the measured shear rate range by a decade toward low shear rates.

We therefore selected the measuring routine from high to low shear rates for further measurements. The reason why the measurement routine from low to high shear rates is error prone in the low shear rate range has not yet been clarified. A possible influence on the measurement could be the protective film used, which is inserted between the polymer and the measurement geometry.

4.4 Verification of the ramp test by the temperature dependence viscosity of the LLDPE and PBD

To further verify the ramp-test method, the lowest viscosity and highest viscosity polymers were tested at different temperatures. The ramp-test method was used to obtain the steady-state shear viscosity $\eta(\dot{\gamma})$ of LLDPE and

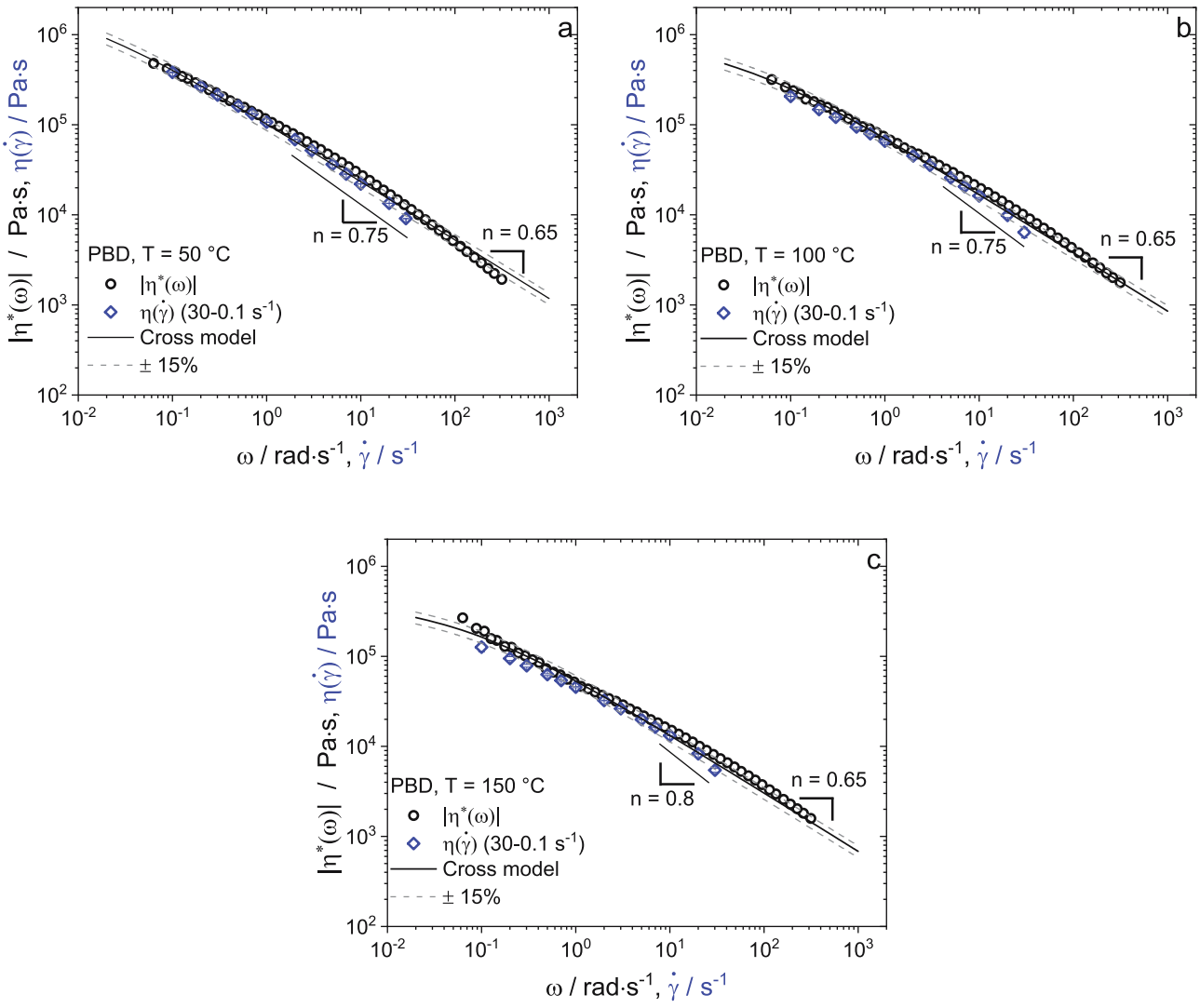

Figure 7: The magnitude of the complex viscosity $|\eta^*(\omega)|$ as a function of angular frequency ω obtained by oscillatory shear frequency sweep experiments with rotational CCR and the steady-state shear viscosity $\eta(\dot{\gamma})$ as a function of shear rate $\dot{\gamma}$ obtained by rotational CCR for PBD at (a) 50°C, (b) 100°C, and (c) 150°C.

PBD at temperatures of T = 140, 160, and 180°C and T = 50, 100, and 150°C, respectively (Figures 6 and 7). TTS of the magnitude of the complex viscosity and the steady-state shear viscosity was investigated. The horizontal a_T and vertical b_T shifting factors were obtained by constructing the master curve using the magnitude of the complex viscosity from SAOS measurements. The same shifting factors were then used to shift the steady-state shear viscosity data obtained by the ramp test (Figures 8 and 9).

Figure 6a–c presents the magnitude of the complex viscosity $|\eta^*(\omega)|$ and the steady-state shear viscosity $\eta(\dot{\gamma})$ of LLDPE at T = 140, 160, and 180°C. At a temperature of T = 140°C (Figure 6a), the steady-state shear viscosity data are below the magnitude of the complex viscosity for the applied shear rate range. Up to a shear rate of $\dot{\gamma} = 10\ s^{-1}$, this deviation is within the 15% deviation of the found Cross model. At temperatures of T = 160°C and T = 180°C, the steady-state shear viscosity data are within the 15% deviation of the corresponding Cross model for the applied shear rate range. On closer inspection, a change in the slope of the steady-state shear viscosity up to a slope of n = 0.6 can be seen for shear rates above $\dot{\gamma} = 10\ s^{-1}$ for all temperatures. It is speculated that this change in slope can be linked to wall slippage, whether we use grooved plates. Heyer et al. have presented similar observations for slippage speculations of high elastic materials with a CCR and grooved plates [18].

For the LLDPE, it can be assumed that the Cox–Merz rule is applicable within a 15% deviation up to the

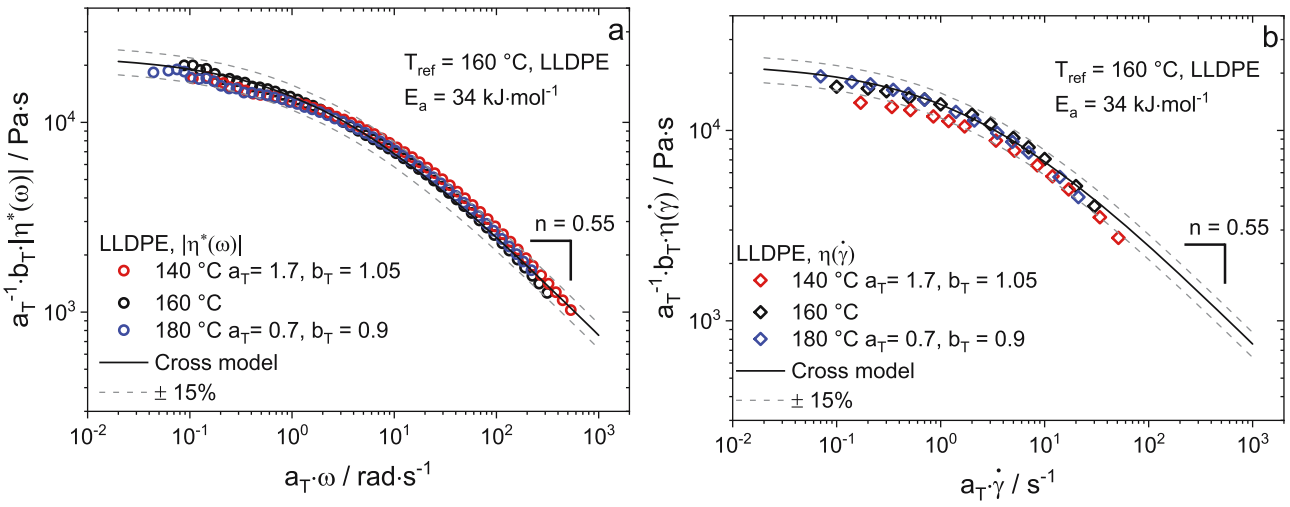

Figure 8: TTS of LLDPE based on results of Figure 6 at a reference temperature of T = 160°C for (a) the magnitude of the complex viscosity $|\eta^*(\omega)|$ and (b) the steady-state shear viscosity $\eta(\dot{\gamma})$.

investigated shear rate of $\dot{\gamma} = 30\ s^{-1}$. These findings are consistent with the results obtained by the capillary rheometer (Figure 3b).

The magnitude of the complex viscosity $|\eta^*(\omega)|$ and the steady-state shear viscosity $\eta(\dot{\gamma})$ for PBD are shown in Figure 7a–c at T = 50, 100, and 150°C. For all temperatures, the steady-state shear viscosity data are below the data of the magnitude of the complex viscosity. Apart from the data for the shear rate of $\dot{\gamma} = 30\ s^{-1}$ for all three temperatures, and the data for the shear rates of $\dot{\gamma} = 0.1–0.3\ s^{-1}$ for a temperature of T = 150°C, the steady-state shear viscosity data are within the 15% deviation of the corresponding Cross model.

Starting at a shear rate of $\dot{\gamma} = 2\ s^{-1}$ for T = 50°C, a shear rate of $\dot{\gamma} = 5\ s^{-1}$ for T = 100°C, and a shear rate of $\dot{\gamma} = 10\ s^{-1}$ for T = 150°C, a decrease in the slope of the steady-state shear viscosity up to a slope of n = 0.75–0.8 can be seen. Even if the data are within the defined 15% deviation, this change in slope indicates that wall slippage may occur, as reported for LLDPE previously.

The data measured at different temperatures were used to generate a master curve by a TTS. A detailed description of this method is given by Mavridis and Shroff [21]. As shown in Figure 8a, the magnitude of the complex viscosity $|\eta^*(\omega)|$ for LLDPE at the different temperatures can be superimposed by shifting them vertically and horizontally, resulting in one master curve. Using an Arrhenius approach, the activation energy can be determined from the horizontal shifting factors $\left(a_T = \left[\left(\frac{E_a}{R}\right)\star\left(\frac{1}{T} - \frac{1}{T_{ref}}\right)\right]\right)$ [21]. For LLDPE, an activation energy E_a = 34 kJ mol^{-1} was found. This value is higher than values reported in the literature, e.g., $E_a \approx 29$ kJ mol^{-1} in the work of Stadler et al. [39] and Keßner et al. [40]. However, an activation energy of E_a = 31 kJ mol^{-1} was reported for the same LLDPE in the previous work by Georgantopoulos et al. [22]. Therefore, it can be assumed that the deviation can be attributed to the instruments accuracy, the number of investigated temperatures, and different molecular characteristics (monomer and additives).

As the steady-state shear data should have the same temperature dependence as the SAOS data, the same horizontal a_T and vertical b_T shifting factors were used for the set of steady-state shear viscosity data [41]. The resulting master curve for the steady-state shear viscosity $\eta(\dot{\gamma})$ is shown in Figure 8b. The superposition of the data of the steady-state shear viscosity confirmed that the temperature dependence is equal for both viscosities measured.

Also for the PBD, the shifting factors found for the SAOS data, shown in Figure 9a, can be used to superimpose the steady-state shear viscosity $\eta(\dot{\gamma})$ data, shown in Figure 9b. The activation energy E_a found for PBD is E_a = 24 kJ mol^{-1}. By using the same horizontal a_T and vertical b_T shifting factors, it is also confirmed for PBD that the temperature dependence is equal for both viscosities measured.

The ability to find the same temperature dependence for two polymers for two different measurement routines shows that the ramp test method from CCR is capable of accurately determining the steady-state shear viscosity. In addition, the TTS can also be used to gather further evidence about the slippage behavior. As no wall slippage occurs in SAOS measurements, shifting factors are found that are not influenced by slippage. If these are used to superimpose the steady-state shear viscosity, a

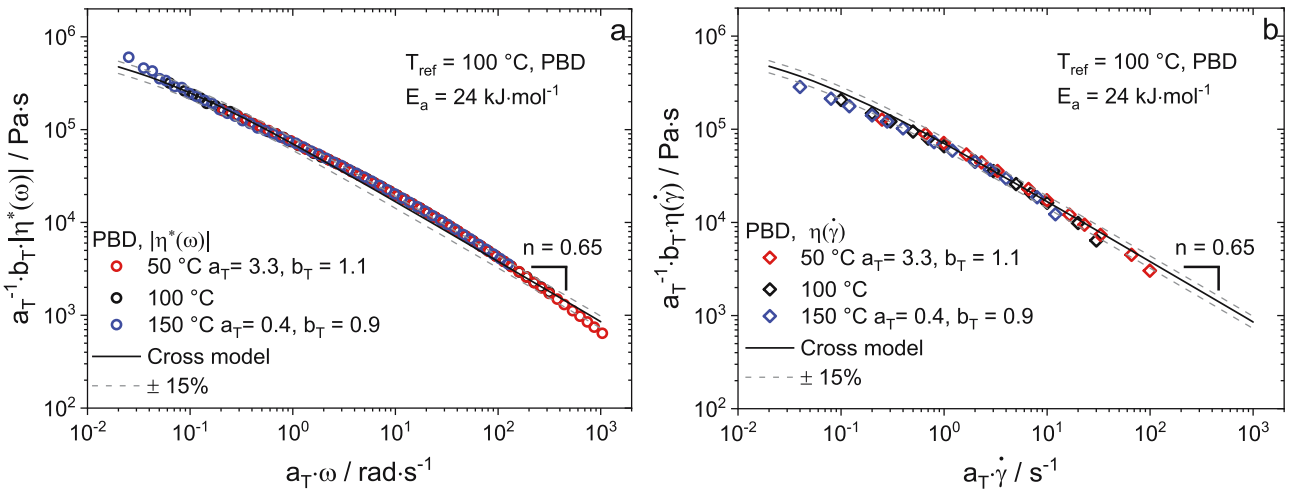

Figure 9: TTS of PBD based on results of Figure 7 at a reference temperature of T = 100°C for (a) the magnitude of the complex viscosity $|\eta^*(\omega)|$ and (b) the steady-state shear viscosity $\eta(\dot\gamma)$.

deviation can be observed at high shear rates, indicating wall slippage.

5 Conclusions

Within this work, we applied and verified the so-called ramp test method, a method used with a CCR to obtain the steady-state shear viscosity $\eta(\dot\gamma)$. By using LDPE, LLDPE, and PBD as model systems, it was shown that the CCR is capable to provide accurate and reliable data in a broad range of temperatures (50–180°C) for low and high viscous materials (M_w = 144 – 375 kg mol^{-1}) over more than 2 decades in shear rate ($\dot\gamma$ = 30 – 0.1 s^{-1}). First, data of the magnitude of the complex viscosity $|\eta^*(\omega)|$ obtained by CCR have been compared to steady-state shear viscosity data obtained by a capillary instrument. Thus, it was shown that the Cox–Merz rule is valid within a 15% deviation for the investigated samples. Subsequently, finite element methods simulations have been performed to investigate the influence of the CCR's sealing on the accuracy of the instrument. By numerical investigations, it was shown that the error due to the sealing cannot exceed 12.2%, and that is only at unlikely conditions of complete no slip at the sealing. Performing the ramp test, the validity of the Cox–Merz rule within a 15% deviation could be confirmed for the three investigated materials. By doing measurements at different temperatures for LLDPE and PBD, it was shown that the CCR is accurate enough to do TTS with SAOS data and with steady-state shear viscosity data. At high shear rates, a decreasing slope of the steady-state shear viscosity became apparent. We speculate that the decreasing slope indicates wall slippage, which has been reported recently [18]. Overall this study shows that CCR can measure steady-state shear viscosity at extrusion-like conditions in a defined manner and through a relatively easy measurement procedure. Beyond that, the ramp test could be used to obtain the steady-state shear viscosity $\eta(\dot\gamma)$ for solvent sensitive materials due to the closed cavity and the regulated pressure.

Acknowledgements: The authors acknowledge support by the KIT-Publication Fund of the Karlsruhe Institute of Technology. The authors thank Henri G. Burhin for the useful discussions and providing the presentation given at the Nordic Rheology Conference 2021. Also, the authors thank Patrick Heyer for the useful discussion and providing the presentation given at the Annual European Rheology Conference 2022. In addition, the authors thank Thomas Rauschmann for providing the presentation for the new RPA Ultra given at the Deutsche Kautschuk Tagung 2021. Further, the authors thank Dr. Michael Pollard for proofreading the manuscript. Felix Ellwanger and M. Azad Emin would like to acknowledge Sandeep Reddy for his help in performing the CCR measurements. In addition, Felix Ellwanger acknowledge support by the state of Baden-Württemberg through bwHPC. Christos K. Georgantopoulos and Manfred Wilhelm would like to acknowledge Prof. Dr. Markus Busch and Ms. Elisabeth Schulz for their help in performing and analyzing the high-temperature SEC experiments for the polyethylene sample, LDPE. In addition, CKG thanks Dr. Andrea Causa for valuable discussions and Pirelli Tyres S. p. A. for financial support during his PhD.

Funding information: This study was partially funded by the Deutsche Forschungsgemeinschaft (DFG, German Research Foundation) project SPP 1934 DisPBiotech.

Author contributions: F.E.: conceptualization (lead); data curation (lead); formal analysis (lead); investigation (lead); and writing – original draft (lead). C.K.G.: conceptualization (supporting); data curation (supporting); formal analysis (supporting); investigation (supporting); writing – original draft (supporting). H.P.K.: supervision (support). M.W.: supervision (support). M.A.E.: conceptualization (supporting); supervision (lead).

Conflict of interest: The authors declare no conflict of interest. The funders had no role in the design of the study; in the collection, analyses, or interpretation of data; and in the writing of the manuscript, or in the decision to publish the results.

Ethical approval: The conducted research is not related to either human or animal use.

Data availability statement: The datasets generated during and/or analyzed during the current study are available with the corresponding author on reasonable request.

References

[1] Kohlgrüber K. Co-rotating twin-screw extruders: Fundamentals. München: Carl Hanser Verlag GmbH & Co. KG; 2019.
[2] Vittorias I, Lilge D, Baroso V, Wilhelm M. Linear and non-linear rheology of linear polydisperse polyethylene. Rheol Acta. 2011;50:691.
[3] Georgantopoulos CK, Esfahani MK, Pollard MA, Naue IFC, Causa A, Kádár R, et al. Derivation of a qualitative model for the spatial characteristic wavelength of extrusion flow instabilities: Investigation of a polybutadiene rubber through capillary, slit and complex geometry extrusion dies. Macromol Mater Eng. 2022;307:2200313.
[4] Hatzikiriakos SG. Wall slip of molten polymers. Prog Polym Sci. 2012;37:624.
[5] Wittek P, Ellwanger F, Karbstein HP, Emin MA. Morphology development and flow characteristics during high moisture extrusion of a plant-based meat analogue. Foods. 2021;10:1753.
[6] Pietsch VL, Bühler JM, Karbstein HP, Emin MA. High moisture extrusion of soy protein concentrate: Influence of thermomechanical treatment on protein-protein interactions and rheological properties. J Food Eng. 2019;251:11.
[7] Guyony V, Fayolle F, Jury V. Die dimensions impact on fibrous plant protein formation during high moisture extrusion. Appl Food Res. 2022;2:100228.
[8] Mezger T. Applied rheology: With joe flow on rheology road. Graz: Anton Paar GmbH; 2021.
[9] Cox WP, Merz EH. Correlation of dynamic and steady flow viscosities. J Polym Sci. 1958;28:619.
[10] Snijkers F, Vlassopoulos D. Appraisal of the Cox-Merz rule for well-characterized entangled linear and branched polymers. Rheol Acta. 2014;53:935.
[11] Winter HH. Three views of viscoelasticity for Cox–Merz materials. Rheol Acta. 2009;48:241.
[12] Wittek P, Walther G, Karbstein HP, Emin MA. Comparison of the rheological properties of plant proteins from various sources for extrusion applications. Foods. 2021;10:1700.
[13] Schreuders FKG, Sagis LMC, Bodnár I, Erni P, Boom RM, van der Goot AJ. Small and large oscillatory shear properties of concentrated proteins. Food Hydrocoll. 2021;110:106172.
[14] Schwab L, Hojdis N, Lacayo J, Wilhelm M. Fourier-transform rheology of unvulcanized, carbon black filled styrene butadiene rubber. Macromol Mater Eng. 2016;301:457.
[15] Burhin HG, Rauschmann T. Viscosity measurement of filled rubber compounds - new insight for error free measurements. Kauts Gummi Kunst. 2021;74:39.
[16] Burhin HG, Rauschmann T, Graf H-J. Wall slip in processing rubber compound revisited. Kauts Gummi Kunst. 2021;74:61.
[17] Burhin HG, Rauschmann T, Graf H-J. New and highly efficient method to measure steady shear viscosity and wall slip of rubber compounds: Closed-boundary rheometer (RPA). Rubber Chem Technol. 2022;95:77929.
[18] Heyer P, Wurm C, Ehrentraut H. Measurement and visualizaton of slip in rubber flow. Seville, ES; 2022. (AERC).
[19] Rauschmann T, Burhin HG, Wirth O, Reddy S. Steady shear viscosity measurements of filled rubber compounds using new enhanced RPA technology. Nürnberg, DE; 2022. (DKT IRC).
[20] Morrison FA. Understanding rheology. New York: Oxford University Press; 2001.
[21] Mavridis H, Shroff RN. Temperature dependence of polyolefin melt rheology. Polym Eng Sci. 1992;32:1778.
[22] Georgantopoulos CK, Esfahani MK, Naue IFC, Wilhelm M, Kádár R. Role of molecular architecture and temperature on extrusion melt flow instabilities of two industrial LLDPE and LDPE polyethylenes investigated by capillary rheology, high-pressure sensitivity slit die and optical analysis. J Appl Polym Sci. 2023;140:6.
[23] Emin MA, Quevedo M, Wilhelm M, Karbstein HP. Analysis of the reaction behavior of highly concentrated plant proteins in extrusion-like conditions. Innov Food Sci Emerg Technol. 2017;44:15.
[24] Bagley EB. End corrections in the capillary flow of polyethylene. J Polym Sci. 1957;28:624.
[25] Rabinowitsch B. Über die viskosität und elastizität von solen. Z Phys Chem. 1929;145:1–26.
[26] Snijkers F, Ratkanthwar K, Vlassopoulos D, Hadjichristidis N. Viscoelasticity, nonlinear shear start-up, and relaxation of entangled star polymers. Macromolecules. 2013;46:5702.
[27] Snijkers F, Vlassopoulos D, Lee H, Yang J, Chang T, Driva P, et al. Start-up and relaxation of well-characterized comb polymers in simple shear. J Rheol. 2013;57:1079.

[28] Avalosse T, Rubin Y. Analysis of mixing in corotating twin screw extruders through numerical simulation. Int Poly Process. 2000;15:117.
[29] Avalosse T. Numerical simulation of distributive mixing in 3-D flows. Macromol Symp. 1996;112:91.
[30] Emin MA, Wittek P, Schwegler Y. Numerical analysis of thermal and mechanical stress profile during the extrusion processing of plasticized starch by non-isothermal flow simulation. J Food Eng. 2021;294:110407.
[31] Leblanc JL, Mongruel A. A thorough examination of a torsional dynamic rheometer with a closed oscillating cavity. Prog Rubber Plast Recycl Technol. 2001;17:162.
[32] Hatzikiriakos SG, Migler KB. Polymer processing instabilities: Control and understanding. Bosa Roca: CRC Press; 2004.
[33] Booij HC, Leblans P, Palmen J, Tiemersma-Thoone G. Nonlinear viscoelasticity and the Cox–Merz relations for polymeric fluids. J Polym Sci Polym Phys Ed. 1983;21:1703.
[34] García-Franco CA. A Note on the elasticity of polymer melts described by primary normal stress difference (N1). Macromol Symp. 2013;325–326:184.
[35] Ansari M, Inn YW, Sukhadia AM, DesLauriers PJ, Hatzikiriakos SG. Wall slip of HDPEs: Molecular weight and molecular weight distribution effects. J Rheol. 2013;57:927.
[36] Hatzikiriakos SG, Dealy JM. Wall slip of molten high density polyethylenes. II. Capillary rheometer studies. J Rheol. 1992;36:703.
[37] Ansari M, Hatzikiriakos SG, Sukhadia AM, Rohlfing DC. Rheology of Ziegler–Natta and metallocene high-density polyethylenes: broad molecular weight distribution effects. Rheol Acta. 2011;50:17.
[38] Snijkers F, Vlassopoulos D, Ianniruberto G, Marrucci G, Lee H, Yang J, et al. Double stress overshoot in start-up of simple shear flow of entangled comb polymers. ACS Macro Lett. 2013;2:601.
[39] Stadler FJ, Gabriel C, Münstedt H. Influence of short-chain branching of polyethylenes on the temperature dependence of rheological properties in shear. Macromol Chem Phys. 2007;208:2449.
[40] Keßner U, Kaschta J, Münstedt H. Determination of method-invariant activation energies of long-chain branched low-density polyethylenes. J Polym Sci. 2009;53:1001.
[41] Markovitz H. Superposition in rheology. J Polym Sci: C Polym Symp. 1975;50:431.